Supporting Information

A macrocyclic receptor containing two viologen species connected by conjugated terphenyl groups

Long Chen,[a] Kate J. C. Lim,[a] Tahkur S. Babra,[a] James O. Taylor,[a] Martin Pižl,[b,c] Robert Evans,[d] Ann M. Chippindale,[a] František Hartl,[a] Howard M. Colquhoun*[a] and Barnaby W. Greenland*[a,e]

[a]Department of Chemistry, University of Reading, Whiteknights, Reading, RG6 6AD, UK; email: h.m.colquhoun@reading.ac.uk

[b] J. Heyrovský Institute of Physical Chemistry, Academy of Sciences of the Czech Republic, Dolejškova 3, CZ-182 23 Prague, Czech Republic

[c] Department of Inorganic Chemistry, University of Chemistry and Technology, Prague, Technická 5, CZ-166 28 Prague, Czech Republic

[d] Aston University Institute of Materials Research, School of Engineering and Applied Science, Birmingham, B4 7ET, UK.

[e] Department of Chemistry, School of Life Sciences, University of Sussex, Falmer, BN1 9QJ, UK; email b.w.greenland@sussex.ac.uk

Contents **Page**

Table S1. A comparison of selected experimental and *in vacuo* DFT calculated bond lengths (Å) and angles (°) for $\mathbf{4}^{4+}$.

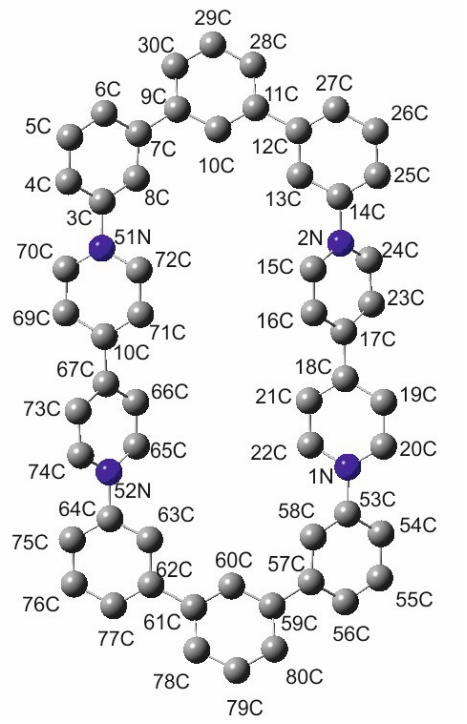

Macrocycle $\mathbf{4}^{4+}$ with atoms numbered (hydrogens removed for clarity).

Bond	Exp.	Calc. *(in vacuo)*
N51-C3	1.451	1.447
N52-C64	1.450	1.447
N1-C53	1.451	1.447
N2-C14	1.450	1.447
N1-C22	1.353	1.349
C22-C21	1.375	1.374
C21-C18	1.368	1.398
C18-C17	1.470	1.484
C17-C16	1.397	1.398
C16-C15	1.355	1.374
C15-N2	1.352	1.349
N52-C65	1.352	1.349
C65-C66	1.355	1.374
C66-C67	1.397	1.398
C67-C68	1.470	1.484
C68-C71	1.368	1.398
C71-C72	1.375	1.374
C72-N51	1.353	1.349

Angle	Exp.	Calc. *(in vacuo)*
N51-C3-C8	118.3	117.7
C3-N51-C72	117.8	118.5
C71-C68-C67	120.5	117.9
C68-C67-C66	120.6	117.9
C65-N52-C64	119.8	118.5
N52-C64-C63	117.8	117.7
N2-C14-C13	117.8	117.7
C14-N2-C15	119.8	118.5
C16-C17-C18	120.6	117.9
C17-C18-C21	120.5	117.9
C22-N1-C53	117.8	118.5
N1-C53-C58	118.3	117.7

Table S2. Comparison of selected DFT calculated (polarizable continuum model, PCM-MeCN) bond lengths (Å) and angles (°) for $\mathbf{4}^{4+}$, $\mathbf{4}^{2(\bullet+)}$ and **4** (for atom numbering see Table S1).

Note the strong variation in the C-N and C-C bond lengths in the heterocycle rings (red entries) for each of the sequential oxidation states of the macrocycle ($\mathbf{4}^{4+}$, $\mathbf{4}^{2(\bullet+)}$ and **4**). In contrast, note the relative invariance with oxidation state of the bond lengths calculated in the polyaromatic spacer units (purple entries). The C-N bonds between the heterocycle rings and polyaromatic spacer units (green entries) also become shorter upon the reduction, which is ascribed to a better π-overlap between C(p) and N(p) orbitals due increasing planarity of the viologen units (Figure 6 in the main text).

	Bond Length (Å)		
Bond	$\mathbf{4}^{4+}$	$\mathbf{4}^{2(\bullet+)}$	**4**
N51-C3	1.442	1.424	1.403
N52-C64	1.442	1.425	1.403
N1-C53	1.442	1.424	1.403
N2-C14	1.442	1.425	1.403
N1-C22	1.350	1.370	1.391
C22-C21	1.373	1.358	1.346
C21-C18	1.395	1.422	1.448
C18-C17	1.473	1.423	1.381
C17-C16	1.395	1.422	1.448
C16-C15	1.373	1.358	1.346
C15-N2	1.349	1.370	1.390
N52-C65	1.349	1.370	1.390
C65-C66	1.373	1.358	1.346
C66-C67	1.395	1.422	1.448
C67-C68	1.473	1.423	1.381
C68-C71	1.395	1.422	1.448
C71-C72	1.373	1.358	1.346
C72-N51	1.350	1.370	1.391
C3-C8	1.386	1.390	1.397
C8-C7	1.395	1.395	1.395
C7-C9	1.476	1.476	1.477
C9-C10	1.395	1.394	1.395
C10-C11	1.394	1.394	1.395
C11-C12	1.476	1.476	1.477
C12-C13	1.395	1.395	1.395
C13-C14	1.386	1.389	1.397
C53-C58	1.386	1.390	1.397
C58-C57	1.395	1.395	1.395
C57-C59	1.476	1.476	1.477
C59-C60	1.395	1.394	1.395

	Bond Angle (°)		
	$\mathbf{4}^{4+}$	$\mathbf{4}^{2(\bullet+)}$	**4**
N51-C3-C8	118.2	119.1	120.1
C3-N51-C72	119.2	120.4	121.4
C71-C68-C67	120.2	122.2	123.4
C68-C67-C66	120.1	122.2	123.4
C65-N52-C64	119.1	120.4	121.3
N52-C64-C63	118.3	119.1	120.0
N2-C14-C13	118.3	119.1	120.0
C14-N2-C15	119.1	120.4	121.3
C16-C17-C18	120.1	122.2	123.4
C17-C18-C21	120.1	122.2	123.4
C22-N1-C53	119.1	120.4	121.4
N1-C53-C58	118.2	119.1	120.1

C60-C61	1.394	1.394	1.395
C61-C62	1.476	1.476	1.477
C62-C63	1.395	1.395	1.395
C63-C64	1.386	1.389	1.397

Table S3. TD-DFT (PBE0/PCM-MeCN) calculated low-lying transitions of triplet $\mathbf{4}^{2(\bullet+)}$ with oscillator strength higher than 0.005 (see Figure S7). Molecular spinorbitals involved in the electronic transitions are depicted in Figures S8 and S9.

Main component (%)	Transition energy [eV] (nm)	Oscillator strength
α-HOSO-1 → α-LUSO (68) α-HOSO → α-LUSO+1 (70)	2.04 (607)	Weak (~0)
α-HOSO-1 → α-LUSO+1 (68) α-HOSO → α-LUSO (68)	2.12 (584)	1.090
α-HOSO-1 → α-LUSO+2 (78) α-HOSO → α-LUSO+7 (35)	2.88 (431)	0.014
α-HOSO → α-LUSO+3 (71)	2.90 (428)	0.137
α-HOSO → α-LUSO+3 (40) β-HOSO-2 → β-LUSO (38) β-HOSO → β-LUSO+1 (49)	2.98 (416)	0.942
β-HOSO-1 → β-LUSO (62)	3.15 (394)	0.035
β-HOSO → β-LUSO+1 (44)	3.16 (392)	0.315
β-HOSO-1 → β-LUSO (64)	3.31 (374)	0.006
β-HOSO → β-LUSO+1 (65) β-HOSO-4 → β-LUSO+1 (45) β-HOSO-5 → β-LUSO (39)	3.33 (373)	0.439
β-HOSO-2 → β-LUSO (76) β-HOSO-5 → β-LUSO (41) β-HOSO-4 → β-LUSO+1 (40)	3.54 (351)	0.058
α-HOSO-1 → α-LUSO+8 (42) α-HOSO-1 → α-LUSO+13 (43) α-HOSO → α-LUSO+9 (48) α-HOSO → α-LUSO+12 (78)	3.60 (344)	0.029
α-HOSO-1 → α-LUSO+8 (57) α-HOSO → α-LUSO+9 (51)	3.61 (343)	0.020
α-HOSO-1 → α-LUSO+10 (78) α-HOSO → α-LUSO+11 (44) β-HOSO-3 → β-LUSO+1 (40)	3.62 (342)	0.013
β-HOSO-7 → β-LUSO (54) β-HOSO-6 → β-LUSO+1 (54)	3.83 (324)	0.13
Mixed	3.98 (312)	0.024
β-HOSO-12 → β-LUSO (59) β-HOSO-11→ β-LUSO+1 (59)	3.99 (311)	0.13
β-HOSO-13 → β-LUSO+1 (66) β -HOSO-14 → β-LUSO (67)	4.06 (305)	0.090

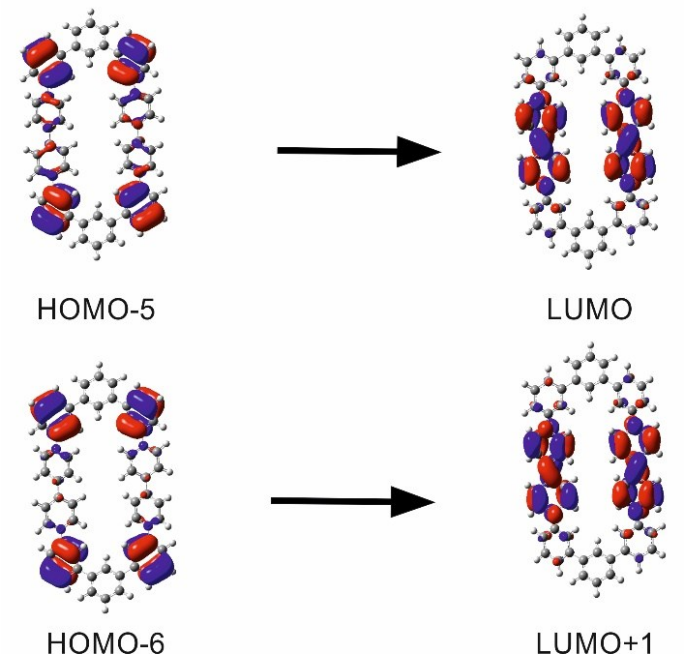

Figure S1. Molecular orbitals of $\mathbf{4}^{4+}$ involved in the calculated transition at 339 nm.

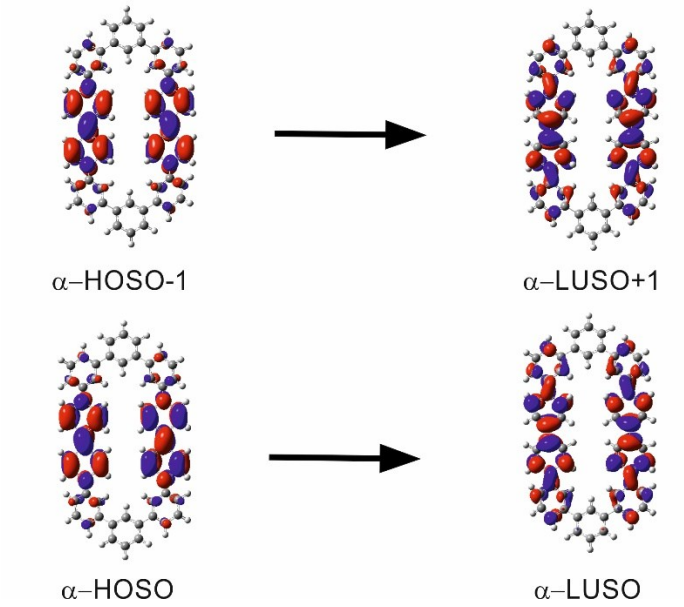

Figure S2. Molecular orbitals of $\mathbf{4}^{2(\bullet+)}$ involved in the calculated transition at 584 nm.

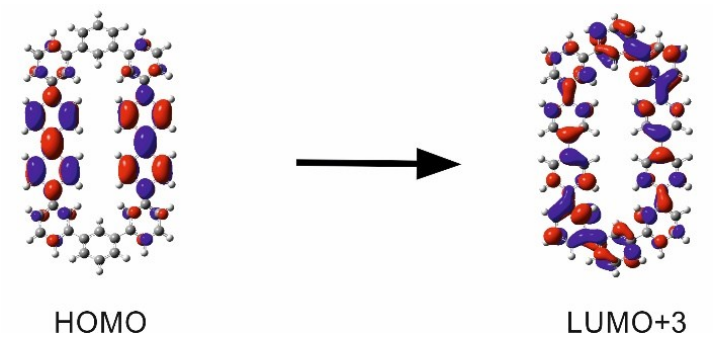

Figure S3. Molecular orbitals of **4** involved in the calculated transition at 453 nm.

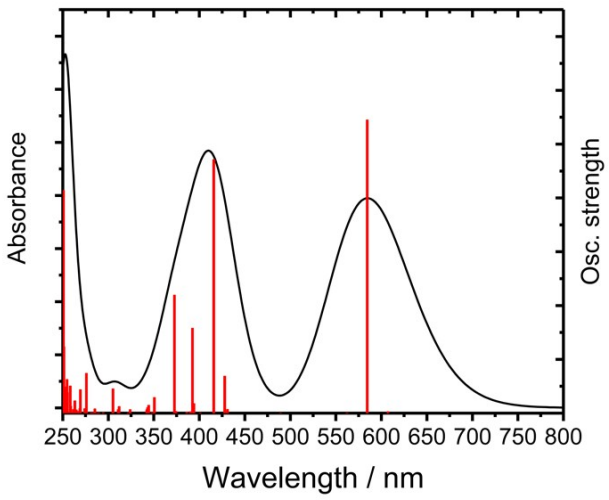

Figure S4. Calculated electronic absorption spectra for $\mathbf{4}^{2(\bullet+)}$ with vertical excitations. (See Table S3 and Figures S5 and S6 for more details.)

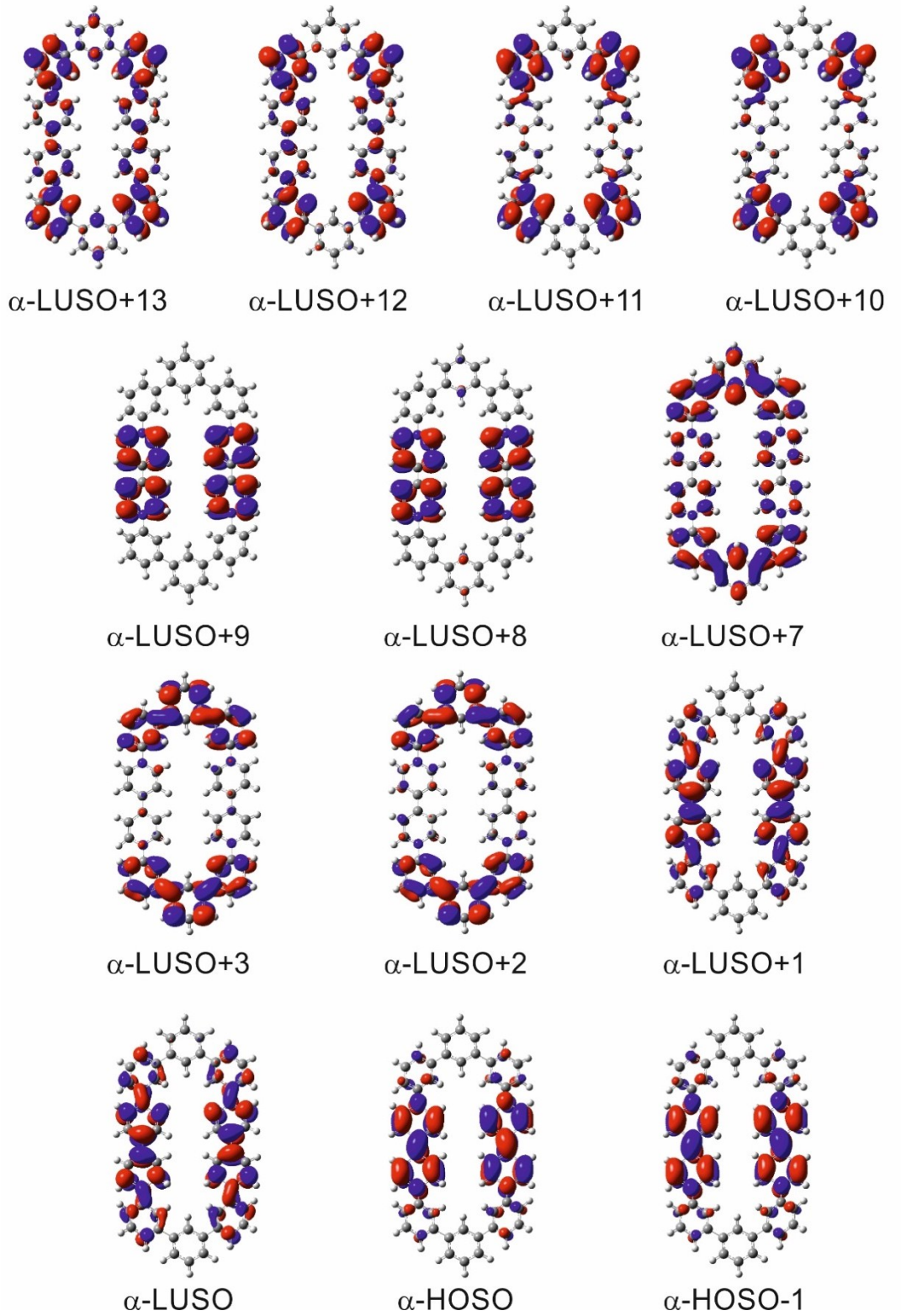

Figure S5. Calculated α-spinorbitals of $\mathbf{4}^{2(\bullet+)}$ involved in the UV-vis electronic transitions (Table S3).

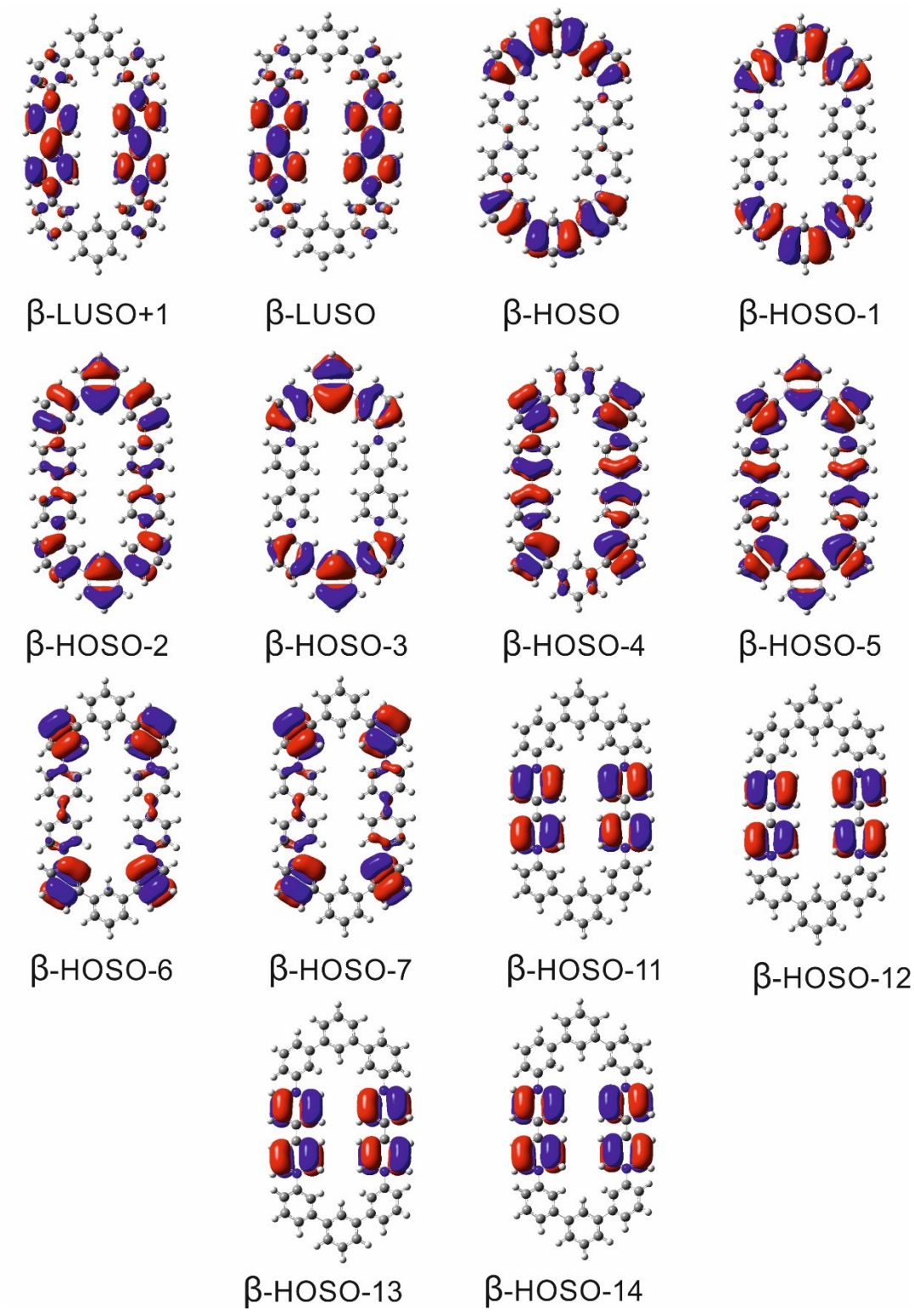

Figure S6. Calculated β-spinorbitals of $\mathbf{4}^{2(\bullet+)}$ involved in the UV-vis electronic transitions (Table S3).

DOSY ^{1}H NMR data

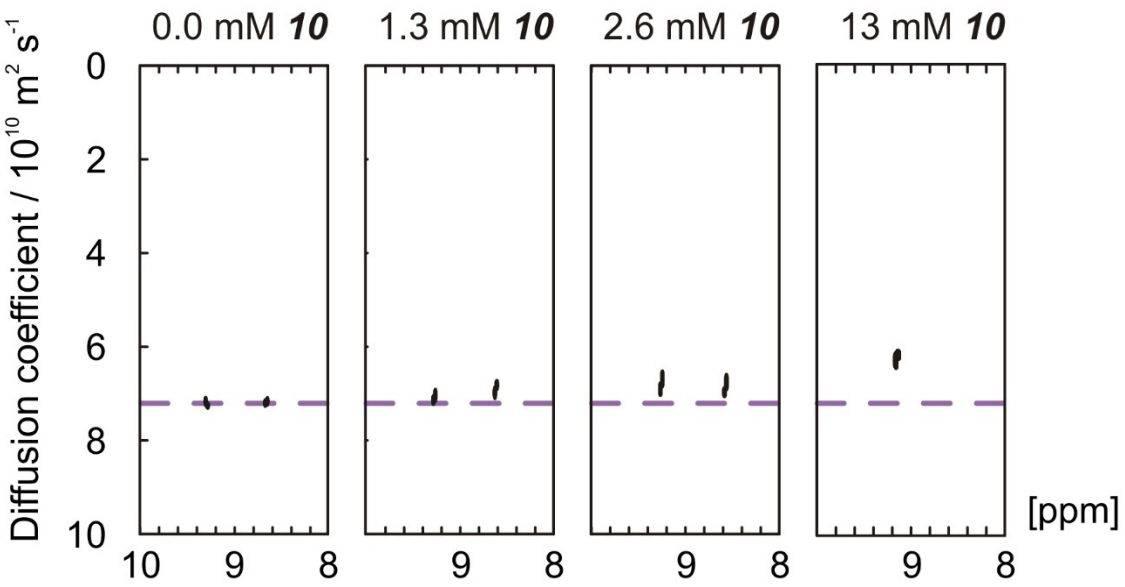

Figure S7. Four DOSY spectra (CD_3CN) corresponding to samples of 1.3 mM **4**$^{4+}$ and 0, 1.3, 2.6 and 13 mM **10** respectively (used to construct Figure 7 in the paper). Only the region between 8 and 10 ppm shown. In the sample containing 13 mM **4**$^{4+}$, peaks at ca. 8.5 ppm are not included in analysis due to overlap of signals from both species. Purple line indicates estimate for diffusion coefficient of **4**$^{4+}$ in the absence of any complexation.

^{1}H and ^{13}C NMR spectra of $\mathbf{4}^{4+}$

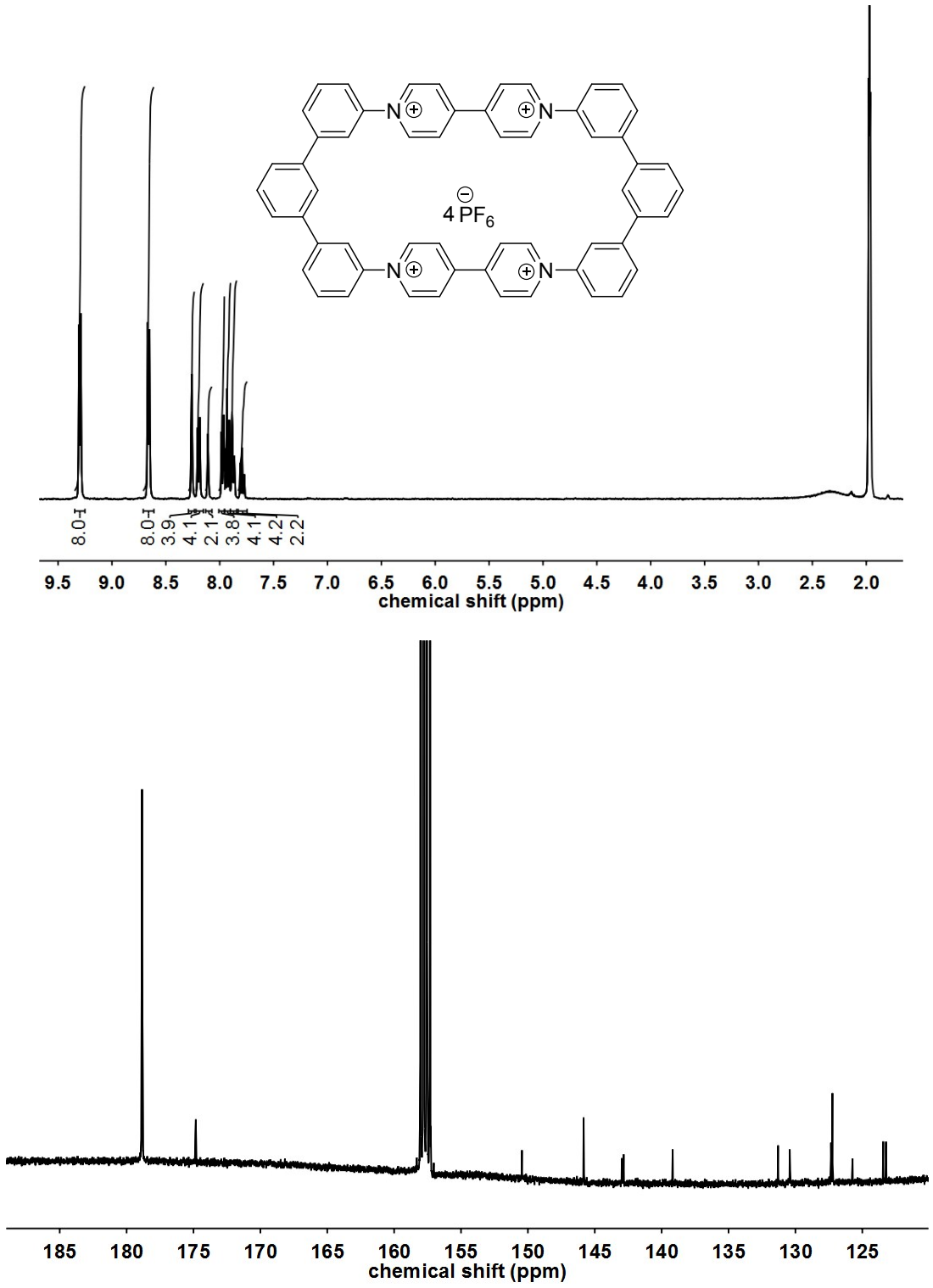

Figure S8. ^{1}H NMR [$(CD_3)_2CO$, 400 MHz] and ^{13}C NMR (CD_3CN, 100 MHz) spectra of $\mathbf{4}^{4+}.4(PF_6^-)$

^{1}H and ^{13}C NMR spectra of **10**

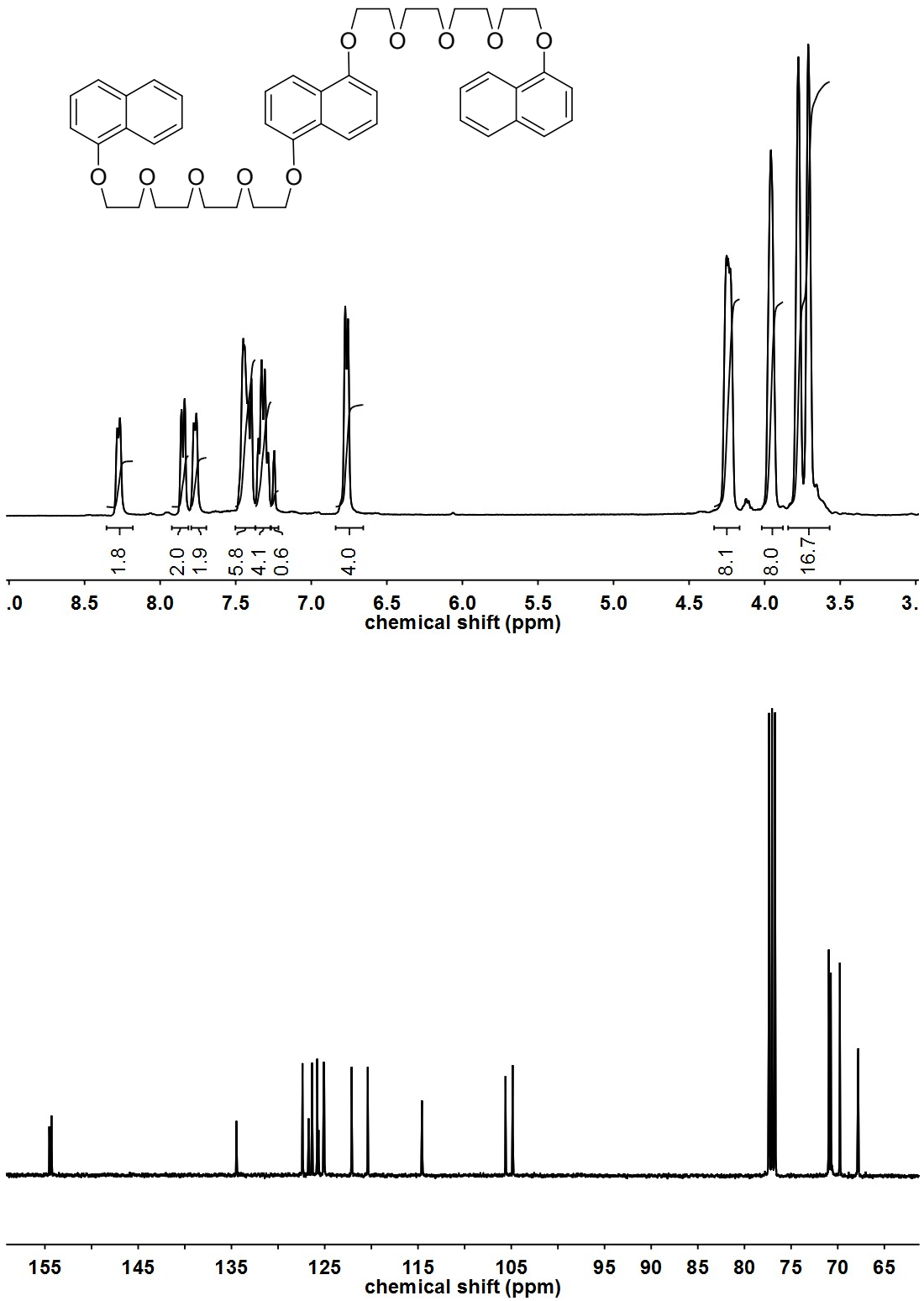

Figure S9. 400 MHz ^{1}H and 100 MHz ^{13}C NMR spectra of **10** ($CDCl_3$)